Scaling and universality in avalanches

Leo P. Kadanoff, Sidney R. Nagel, Lei Wu, and Su-min Zhou
The James Franck Institute and The Department of Physics, The University of Chicago, Chicago, Illinois 60637
(Received 27 December 1988)

We have studied various one- and two-dimensional models in order to simulate the behavior of avalanches. The models are based on cellular automata and were intended to have the property of "self-organized criticality" proposed by Bak, Tang, and Wiesenfeld [Phys. Rev. Lett. **59**, 381 (1987); Phys. Rev. A **38**, 384 (1988)]. By varying the sizes of the systems, we have investigated the scaling properties of these models. In particular, we have addressed the question as to whether simple finite-size scaling or multifractal analysis is more suited to fitting the data on the distribution of avalanche sizes. By varying the underlying microscopic rules that describe how an avalanche is generated, we have also studied whether different models have the same, universal properties. In our one-dimensional models we find that the multifractal analysis is much better than the analysis based on simple finite-size scaling. We also find that there are several different universality classes. Nevertheless, certain models with similar rules appear to belong to the same class. In two dimensions, we find that the simple finite-size scaling works quite well and that the distribution functions can be fit over wide ranges by a simple power law. The multifractal analysis also works well and it is difficult to tell which form is a better fit to the data. Again, as in one dimension, there are several different universality classes and different models with similar rules belong to the same class.

I. INTRODUCTION

In a recent investigation of extended dissipative dynamical systems, Bak, Tang, and Wiesenfeld[1,2] introduced the notion of self-organized criticality. They showed that such dynamical systems naturally evolve into a "critical state" through a self-organization process. This critical state is characterized by no intrinsic length or time scales. They suggested that long-range temporal correlations with a "$1/f$" power spectrum could be understood in terms of self-organized criticality and that there is a connection between "$1/f$" noise and the spatial self-similar fractal structure of the critical state. By analogy with traditional critical phenomena it was argued that near the critical state there is universal behavior and that the systems can be characterized by several critical indices. Bak, Tang, and Wiesenfeld suggested that sandpiles were a particularly clear example of a self-organized system. Sandpiles are built up by randomly adding sand to the system until unstable sand slides off. They argued that the slope of the sandpile in this way will automatically reach a critical value. The corresponding self-organized critical state is an attractor for the dynamics of the system.

In this paper, we simulate a number of simple dynamical systems which may be used to model avalanches in both one and two dimensions. These models are cellular automata in which the basic variable is $h(\mathbf{i})$, where $\mathbf{i}$ is a d-dimensional spatial index and h is an integer variable giving the height of the pile at a given point. Recent experiments[3] have examined the assertion that real sandpiles behave in a critical manner at the angle of repose. No critical behavior was observed in those experiments. The models we will study in this paper thus do not simulate sandpiles but instead are intended to investigate various examples of self-organized criticality.

The models we have investigated all involve two kinds of steps. First, a particle is added to a random site $\mathbf{i}$ and then

$$h(\mathbf{i}) = h(\mathbf{i}) + 1 \ . \tag{1.1}$$

Second, after the addition, a set of cellular automaton rules are applied which give an algorithm for determining whether the slopes of the pile are so large that a slide will occur and exactly how the pile will rearrange itself. These rules are applied repeatedly until all the slopes are sufficiently small at which point the cascade (or avalanche) will cease. The criteria which determine what is stable and the rules for how an unstable pile will reorganize itself until it regains stability will depend on the particular rules of the model. However, all the models we have studied have certain common features. A grain, if unstable, will move to nearby sites. If it reaches a boundary it will drop off the edge. We have examined two different distribution functions. For each avalanche, we calculate the number of grains that drop off the edge D and the total number of flipping events F. For each quantity we can obtain the distribution of such events for systems of different linear size L. The distribution functions $\rho(D,L)$ and $\rho(F,L)$ vary from one model (that is, a set of rules governing how an unstable state may reorganize) to another.

Since our simulations are always on systems of finite size, it is important that we understand how this finite size affects the properties we measure. Thus we are interested in applying the techniques of finite-size scaling to our data. In the finite-size-scaling analysis,[4,5] we fit $\rho(X,L)$ (where X is D or F) via the form

$$\rho(X,L) = L^{-\beta} g(X/L^{\nu}) \quad \text{for } X,L \gg 1 \ . \tag{1.2}$$

Here β and ν are critical indices describing the probability, and g is called a scaling function. This fit works for several of our models. However, for other models we have to use a multifractal fitting form[6-8]

$$\log_{10}\rho(X,L)/\log_{10}(L/L_0) = f(\log_{10}(X/X_0)/\log_{10}(L/L_0)) . \quad (1.3)$$

In the usual notation[7,8] the quantity $\log_{10}(X/X_0)/\log_{10}(L/L_0)$ is called α and the fit (1.3) is called an f-α representation. Here L_0 and X_0 are constants which give the appropriate units of the length and the quantity X. The two forms (1.2) and (1.3) only agree for the case in which g is a simple power law and f is a linear function. Then the entire probability is described by only two scaling indices. Otherwise, there is a whole spectrum of scaling indices, i.e., all the values taken on by $df/d\alpha$. One of the major questions of this paper is when we might expect each of these forms to apply.

Universality[9,10] is the statement that two different problems in the critical regime ($L \gg 1, X \gg 1$) may have the same critical behavior. A universality class is a set of problems for which the behavior is the same. We can test universality by looking at the critical indices and the functions f or g and seeing whether they are indeed the same for the different problems. Our goal is to elucidate the extent of universality for these dynamical problems.

Before we launch into the analysis, we should explain why we think that these models are interesting. These models are very simple and accessible examples of time-dependent systems in which there is a kind of scale-invariant behavior automatically generated by the dynamical process. In understanding these systems we might gain an insight into dynamical processes in real systems.

However, the reader might ask how we know *a priori* that there is some scale-invariant behavior in these models. Might we not have a trivial situation in which the $\rho(X,L)$ are simply peaked at small values of X and have an uninteresting L dependence? Not so. It is true that, for small X, $\rho(X,L)$ has a nonuniversal structure in which there is a likelihood of order unity of small-X events. However, by the nature of the process $\rho(X,L)$ must have some weight for large X. To see this, consider the probability $\rho(D,L)$ that D grains will fall off the edge in a given avalanche. For $D=0$, $\rho(D,L)$ is close to unity and for small D falling events have a likelihood of order $1/L$

$$\rho(D,L)=c(D)/L \quad \text{for } D=1,2,\ldots \quad (1.4)$$

since the most likely fall events occur when a particle is added near the edge. For small D this structure is nonuniversal and not scale invariant. However, since the pile is in a kind of steady state, on the average one grain must fall for each grain added. In symbols

$$\sum_D \rho(D,L)D = \langle D \rangle = 1 . \quad (1.5)$$

Equations (1.4) and (1.5) can only coexist if $\rho(D,L)$ has some weight for D of order L and hence a nontrivial scaling structure. The same argument can be extended to show that $\rho(F,L)$ also has a nontrivial scaling structure. This is an indication that events which involve large values of D and F must play an important role in determining the steady-state dynamics of avalanches.

The paper is organized as follows: In Sec. II, we will introduce several one-dimensional models which show nontrivial behavior. We discuss the finite-size scaling and multifractal structure in these models and we compare results between the models. We extend our work to the two-dimensional case in Sec. III and discuss the dependence of our results on the symmetry of the models. In Sec. IV we summarize our results.

II. ONE-DIMENSIONAL AVALANCHE SIMULATIONS

A. The models

We begin our discussion of landslides with the models that are spatially one dimensional. To simplify the calculation, we assume integer heights $h(i)$ at lattice sites $i=1,2,3,\ldots,L$, where L is the size of system. The local slope of the pile $\sigma(i)$ at site i is defined as the height difference between two nearest neighbors

$$\sigma(i)=h(i)-h(i+1) . \quad (2.1)$$

The boundary conditions are such that grains can flow out of the system from the right side only. This corresponds to a closed boundary at the left edge and an open boundary at the right edge:

$$\sigma(0)=0 , \quad (2.2a)$$

and

$$h(i)=0 \quad \text{for } i>L . \quad (2.2b)$$

To start the cascade we add particles according to Eq. (1.1) with i chosen randomly in the range $1-L$. Then the avalanche can start. In each step of the avalanche, we examine the system to see whether a slide can occur. This can happen at site i if

$$\sigma(i)>\sigma_c . \quad (2.3)$$

At all sites which satisfy the condition (2.3) we construct in parallel a decrease in $h(i)$ and an increase in $h(i+1)$, $h(i+2),\ldots,$ with the condition that the decrease in $h(i)$ is equal to the increase in the other sites. Increases which would have involved $i>L$ are called drops and the corresponding h's are reset to zero. Notice that, except for the grains which fall off the end, the number of grains is conserved. Thus the models involve a kind of nonlinear diffusion.

The simplest one-dimensional dynamical rule was introduced by Bak, Tang, and Wiesenfeld.[1] In this model, the pile just builds up and reaches a "least-stable state" where all the height differences are equal to the critical value $\sigma(i)=\sigma_c$. Any additional particles dropped onto the system will slide from site to site until they reach the boundary and leave the system. Since particles are added at random sites, all values of F between 1 and L are equally likely. The only possible value of D in this least-stable state is 1. The probability distribution for D has its entire weight at D equal to 1, and hence has no scaling

behavior. For F a fit of the form (1.2) (finite-size scaling) or (1.3) (multifractal) is equally appropriate. In the finite-size-scaling fit $\beta_F=1$, $\nu_F=1$, and

$$g(x)=\begin{cases}1 & \text{for } x\le 1\\ 0 & \text{for } x>1\ .\end{cases} \tag{2.4}$$

Alternatively the multifractal fit gives

$$f(\alpha)=\begin{cases}-1 & \text{for } \alpha\le 1\\ -\infty & \text{for } \alpha>1\ .\end{cases} \tag{2.5}$$

Other one-dimensional models can be devised which show nontrivial behavior in that the distribution functions $\rho(D,L)$ and $\rho(F,L)$ have a complicated dependence on their arguments. The models which we will consider in this section differ in two separate regards: They can be either local or nonlocal and can be either limited or nonlimited. All the models have particles dropping from the site i as

$$h(i)\to h(i)-n_f(i)\quad\text{(all models)} \tag{2.6}$$

whenever condition (2.3) is satisfied. Here $n_f(i)$ is the number of grains which move to the right from site i. In the limited models $n_f(i)$ is limited to have a constant value

$$n_f(i)=N_F\quad\text{(limited models)}\ . \tag{2.6a}$$

In contrast, in the unlimited models the number of grains which slides grows in proportion to the slope

$$n_f(i)=\sigma(i)-N_S\quad\text{(unlimited models)}\ . \tag{2.6b}$$

These two kinds of models turn out to be very different. In the unlimited case there is a tendency to build up a very tall wall (proportional perhaps to a power of L) and have that wall slide downward step by step.

What will happen will be further determined by the choice of whether the model is local or nonlocal. In the local case, all the grains slide down onto the next site and the flow is described by Eq. (2.6) and

$$h(i+1)\to h(i+1)+n_f(i)\quad\text{(local models)} \tag{2.7a}$$

for all i values which have the slide condition (2.3) satisfied. In the nonlocal case the stack "falls over" and adds one grain to each downhill site so that in addition to Eq. (2.6) one has

$$h(i+j)\to h(i+j)+1\quad\text{for } j=1,2,\ldots,n_f(i)$$
$$\text{(nonlocal models)}\ . \tag{2.7b}$$

Given these definitions, there are two parameters in each model: σ_c, which determines when the slide events will occur, and N_F (or N_S), which determines exactly how many grains will slide in each event for the limited (or unlimited) cases. However, in this one-dimensional example σ_c is completely irrelevant since it will only determine the average value of $\sigma(i)$.

All of the models discussed above can be described most conveniently in terms of the changes that the various processes induce upon $\sigma(i)$. For example, adding a grain at i changes the σ's by adding 1 to $\sigma(i)$ and subtracting 1 from $\sigma(i-1)$. [Of course, the subtraction does not occur if $i=1$ since $\sigma(0)=0$ is the boundary condition.] Similarly, the slides can be described by writing that a slide produced by a too-large slope at i has

$$\sigma(j+i)\to\sigma(j+i)+X_i(j)\ . \tag{2.8}$$

For example, in the local limited model, the change $X(j)$ is given by

$$X_i(-1)=X_i(1)=N_F,\quad X_i(0)=-2N_F\ , \tag{2.9a}$$

for i not equal to 1 or L. For these two exceptional cases

$$X_i(1)=N_F,\quad X_i(0)=-2N_F\quad\text{for } i=1\ , \tag{2.9b}$$

while

$$X_i(-1)=-X_i(0)=N_F\quad\text{for } i=L\ . \tag{2.9c}$$

All the X's not explicitly mentioned in Eqs. (2.9) are zero.

B. Conservation laws and sum rules

We have already noticed that there is a conservation law for the total number of particles so that in any cascade the quantity D plus the total mass

$$M=\sum_i h(i)$$

remains unchanged. Since the model can be completely expressed in terms of the slopes $\sigma(i)$ we rewrite the sum rule in terms of the same quantity. Notice that σ and h are related by

$$h(i)=\sum_{j=i}^{L}\sigma(j)\ , \tag{2.10}$$

so that M is alternately given by

$$M=\sum_i i\sigma(i)\ . \tag{2.11a}$$

The formal derivation of the conservation law from Eq. (2.11) involves going back to Eq. (2.6) and noticing that the sum

$$\sum_j (i+j)X_i(j)$$

represents the total change in M produced by the slide at i. Then the conservation law is the statement that this moment of X vanishes except for the "exceptional cases" in which i is sufficiently large so that particles fall off the end. [See Eq. (2.9) for a specific example which fits this rule.] Other sum rules follow from other moments of the "change vector" X. For example, the total σ

$$\sigma_T=\sum_i\sigma(i) \tag{2.11b}$$

also obeys a conservation law. This quantity is just $h(1)$. Consequently, the only slides that can change the value of σ_T have $i=1$. This is expressed in the moment condition:

$$\sum_j X_i(j)=0 \quad \text{for } i\neq 1 \ .$$

There is one more interesting moment of $\sigma(i)$,

$$H=\sum_i i(L-i)\sigma(i) \ . \tag{2.11c}$$

Since each slide involves grains which move toward higher values of i, this quantity tends to be decreased by the motion of particles. However, when particles fall off the end, H increases. To see this in detail, one calculates the change in H due to each slide by looking at the corresponding moment of X. For example, in the local, limited model Eq. (2.9) implies that

$$\sum_j (i+j)(L-i-j)X_i(j)=\begin{cases}-2N_F & \text{for } i\neq L\\ (L-1)N_F & \text{for } i=L \ .\end{cases}$$

It then follows that during a cascade of slides

$$H\rightarrow H-(2N_F)F+(L+1)D \ . \tag{2.12}$$

Here F is the number of slide events. On the average, addition events have no effect upon H. By using the sum rule (1.5) and the fact that H must, in the long run, remain constant, we find another sum rule:

$$\langle F\rangle=\sum_F F\rho(F,L)=(L+1)/(2N_F)$$

$$\text{(limited, local model)} \ . \tag{2.13}$$

This sum rule is an indication that the flip number should have an interesting scaling structure.

Equation (2.12) directly shows a decrease in H from flips F and an increase from drops D. But consider the quantity

$$S=-H-M(L+1) \ .$$

From the sum rule on M, one sees that during each slide S increases continuously. This behavior of S is important because it shows that the avalanche has a preferred direction in time toward higher S. The slide cannot go on forever; eventually S will increase so far that further slides will not take place.

We can also deduce some relations between the finite-size-scaling exponents using the sum rule (2.13),

$$\begin{aligned}(L+1)/(2N_F)&=\sum_F F\rho(F,L)\\ &=\sum_F FL^{-\beta_F}g(F/L^{\nu_F})\\ &=\int dF\,FL^{-\beta_F}g(F/L^{\nu_F})\\ &\sim L^{2\nu_F-\beta_F} \ .\end{aligned}$$

In this way we conclude that as long as the integral converges

$$\beta_F=2\nu_F-1 \quad \text{(in the limited, local model)} \ . \tag{2.14}$$

Similarly for the drop number

$$1=\langle D\rangle=\int dD\,DL^{-\beta_D}g(D/L^{\nu_D})\sim L^{2\nu_D-\beta_D}$$

and

$$\beta_D=2\nu_D \quad \text{(all models)} \ . \tag{2.15}$$

C. Universality and scaling in one dimension

The questions that we are interested in studying are whether the different models described above have scaling or multifractal behavior and whether that behavior is universal between different models. Our general conclusions are as follows. Simple finite-size scaling does not work well for the data on these one-dimensional models. Instead we find that the multifractal analysis, represented by Eq. (1.3), gives a satisfactory fit to the data in all cases. Each of the four categories of models we have discussed above falls into different universality classes. However, we have found that at least in one of these categories, the one with limited local rules, two different models appear to belong in the same universality class.

In order to arrive at these conclusions we have had to analyze our data in some ways which may not be obvious *a priori*. In the rest of this section we will describe in detail the variety of behaviors we have observed and give the details of how our analysis was performed.

1. Limited models

The most simple of the models that we will discuss are the limited, local ones where a fixed number of grains N_F fall to a nearest neighbor during each step of an avalanche. We first examine the distribution of drops $\rho(D,L)$ when $N_F=2$. In Fig. 1(a) we show the raw data for seven system sizes with L ranging from 32 to 2048. Our first attempt will be to see if this data can be fit with the scaling behavior form (1.2). We try to shift the origin of the curves on a log-log plot until the distributions for different values of L lie on top of one another. The shift of the ordinate gives the value of β_D while the shift of the abscissa gives ν_D. Such a fit to the data is shown in Fig. 1(b). We see that the curves lie approximately on top of one another only in the region of relatively small D. This fit works poorly for the data in the large-D region where different scaling exponents are needed to get an adequate fit. Clearly, one set of exponents is not sufficient to fit the data at both large and small values of D.

We next try a multifractal fit (1.3) to the same data. We have plotted $\log_{10}\rho(D,L)/\log_{10}(1.5L)$ against $\log_{10}(D/N_F)/\log_{10}(1.5L)$ (where, for this model, $N_F=2$) for the different size systems. (1.5) and N_F represent our best fits for the constants L_0^{-1} and X_0 in Eq. (1.3). The large-L results are insensitive to the exact values chosen. A good fit is represented by having all the points for different L values fall on the same curve. This type of fit is shown in Fig. 1(c). In order to emphasize the excellent quality of our fit we have omitted the first five points from each of our curves which is the only place where the curves did not lie on top of one another. We would not necessarily expect these points to have any scaling behavior since they are determined by the microscopic nature

of the rules.

Before turning our attention to the flip-number distribution for this model we will examine the behavior of $\rho(D,L)$ for another limited, local model, this time with $N_F=20$, to show that we get similar behavior as for the case just described ($N_F=2$). The multifractal fit is shown in Fig. 1(d). We see that all the curves for different values of L fall on top of one another. Moreover, we see that the shape of the curve is the same as for the $N_F=2$ model. The inset in this figure shows the data for both models superimposed. It is clearly difficult to tell these curves apart.

In order to examine the question of the universality of these two models more carefully we now turn our attention to the distribution of flips $\rho(F,L)$. In Fig. 2(a) we show the data for $\rho(F,L)$ for the seven sizes of L studied. If we try a simple scaling fit we find that there are at least two regions with different scaling functions: $F<L$ and $F\gg L$. These are shown in Figs. 2(b) and 2(c). In the small-F regime $\beta_F=0.38\pm0.05$ and $\nu_F=0.34\pm0.05$ which is inconsistent with the sum rule (2.14). Both the fact that there are at least two different scaling regions and the fact that (2.14) is not satisfied in one of the regions suggests that a simple scaling interpretation of the data is not adequate.

As in the case of the distribution of drops, this data can be fit more satisfactorily with the multifractal form as is shown in Fig. 2(d). However, even here we find that the data at relatively low values of F do not lie on top of one another for different system sizes L. As the size of the system increases the curves do look as if they are approaching an asymptotic curve but they approach this limit slowly (roughly logarithmically). In order to convince ourselves that the multifractal fit is good, we have to examine the model in detail in order to discover what microscopic effect is the cause of this discrepancy.

The mechanism responsible is a rather subtle one, and we explain it here only because it is important to our argument about multifractal fitting and to the question of universality between the $N_F=2$ and $N_F=20$ models. When a particle is added at the site i an avalanche can start that will travel in two directions. Of course the first event must be that N_F particles (the added particle and N_F-1 particles which were already on the pile) fall "downhill." This event, however, can leave the site at $i-1$ unstable. This backward, "uphill" motion of the avalanche is the source of our problems with the multifractal fit. The dynamics for the *start* of the backward motion is subtilely different from the dynamics involved when the backward avalanche has gone more than one

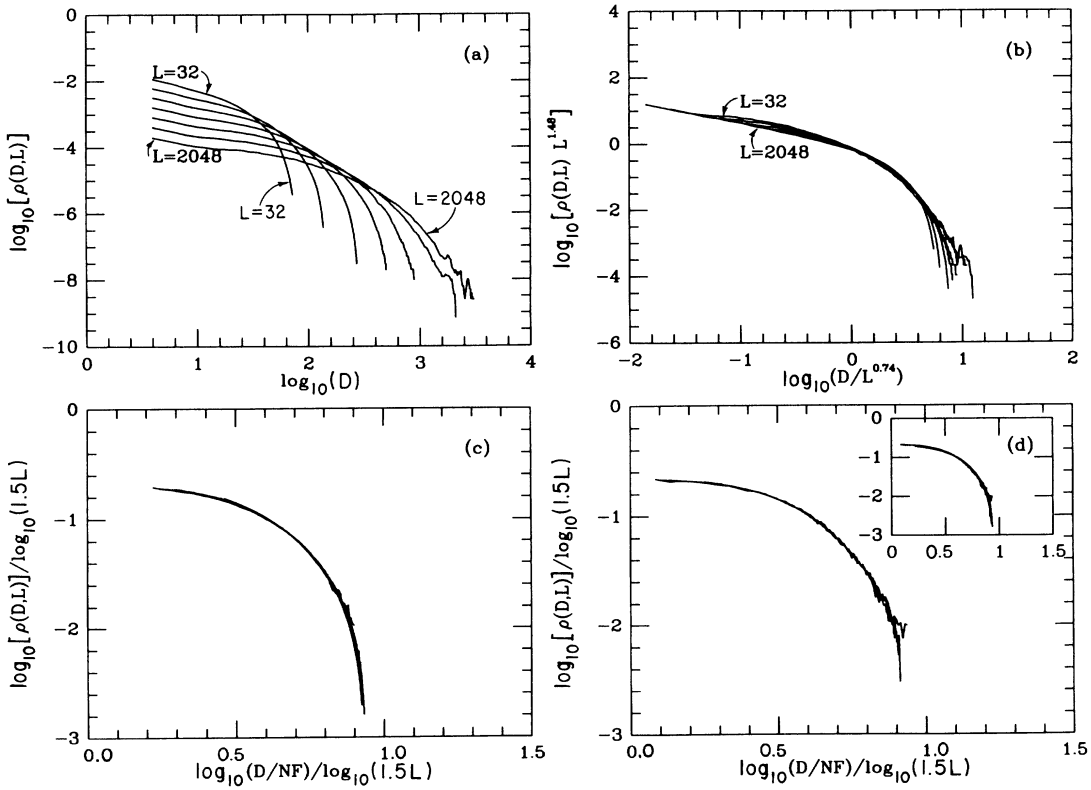

FIG. 1. (a) Distribution of drop number $\rho(D,L)$ for seven system sizes with L ranging from 32 to 2048 for the limited, local model with $N_F=2$. (b) A finite-size-scaling fit for the same data. The scaling exponents used in this plot are $\nu_D=0.74$ and $\beta_D=2\nu_D=1.48$. (c) The plot of f vs α for the same data. Note that the fit is much better than simple finite-size scaling. (d) The plot of f vs α for the limited local model with $N_F=20$. The system sizes range from 128 to 2048. The inset in this figure shows the data for the $N_F=2$ and $N_F=20$ models superimposed.

step. To see this we note that when the site i is unstable only N_F-1 of the original particles on the pile leave that site. Thus the site at $i-1$ is slightly more stable than at another site farther up the hill where if the particle in front of it had been unstable N_F particles would have fallen. Clearly this slight difference between the first and second backward steps up the pile will decrease as N_F increases.

In Fig. 3(a) we plot the data for $\rho(F,L)$ with the data removed which corresponds to 0 or 1 backward steps of the avalanche and find that the multifractal form gives an excellent fit to the data. (The simple finite-size scaling does not work appreciably better than it did without the removal of this data.) In Fig. 3(b) we plot all the data (i.e., with no data taken out) for the $N_F=20$ model. It is clear that, just as we suggested in the last paragraph, for large values of N_F the multifractal fit works well without having to take the backward dynamics into account. We also note that we have only removed those data points which correspond to the first two events of its kind *independent* of the *size* L. Thus we do not believe that we have removed any data which could reasonably have been expected to be in the scaling regime. Finally in the inset to Fig. 3(b) we show the data for $\rho(F,L)$ (with the appropriate back steps removed) for the $N_F=2$ and $N_F=20$ models superimposed on one another. The coincidence of the two sets of data is again convincing evidence that these two models are in the same universality class. Moreover, the fact that the raw data itself are not identical shows that these two models are not trivially the same.

The data for the limited nonlocal model show a behavior similar to that found in the local case. In Fig. 4(a) we show the multifractal fit for $\rho(D,L)$. Again this fit works much better than does a simple scaling form. In Fig. 4(b) we show the multifractal fit for $\rho(F,L)$ in the same model. Again the fit works well for the large values of F but significant discrepancies arise at smaller values which are reminiscent of what we found in the local case. A similar analysis, where one removes the data with zero and one backstep of the avalanche, is shown in the inset. As in the limited, local model, it again shows a good multifractal fit over the entire range of the data.

We are hesitant to claim that the nonlocal models are in the same universality class as the local ones. When we look at the nonlocal models for $N_F=20$ we find that the behavior has changed considerably from that with $N_F=2$. Also we find that a superposition of the $N_F=2$ data for the local and nonlocal cases, although reasonable, does not work as well as it did for the $N_F=2$ and $N_F=20$ local models.

2. *Unlimited models*

The multifractal fits for $\rho(D,L)$ for the unlimited local and nonlocal models are shown in Figs. 5(a) and 5(b), respectively. For the local model we have again found that

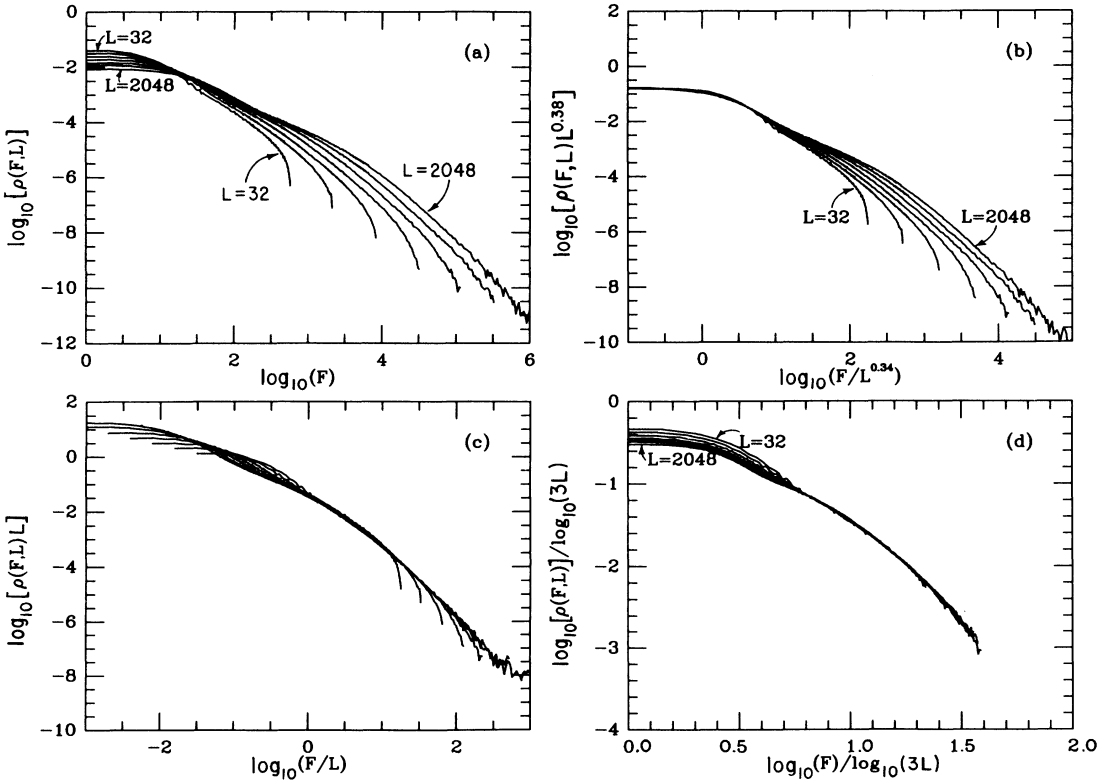

FIG. 2. (a) Distribution of flips in the limited local model with $N_F=2$ for seven system sizes with L ranging from 32 to 2048. (b) and (c) Finite-size-scaling fit for two different sets of exponents. A simple finite-size scaling is not an adequate fit to the data over the entire range of F. (d) Plot of f vs α for the same data shows that the multifractal form gives a more satisfactory fit.

a better fit could be obtained if we remove the data that correspond to the first two steps of an avalanche moving backwards up the hill. In neither case did the finite-size-scaling analysis give an adequate fit to the data.

The distribution function $\rho(D,L)$ can be fit approximately by

$$\rho(D,L)\approx D^{-\delta_D}\exp(-D/L)\ . \tag{2.16}$$

In the case of the local model $\delta_D=1.66$ and in the case of the nonlocal model $\delta_D=0.87$. We therefore conclude that these models lie in different universality classes from each other and in different classes from the limited models.

If we now turn our attention to the distribution of flips $\rho(F,L)$ we again find that simple scaling does not work at all. First we examine the local model. Figure 6(a) shows $\rho(F,L)$ for seven systems with L between 32 and 2048. For each value of L there is a ragged region for small F, and a power-law behavior for F higher than about 12. The power law terminates in a bump, which is followed by another apparent power law, and finally a very rapid falloff of $\rho(F,L)$ at the highest F values.

There are two scaling fits which look good over limited ranges of the data: one for low and intermediate values, where $\beta_F=\nu_F=0$ [Fig. 6(a)], and the other for higher values of F, where $\beta_F=2.4$ and $\nu_F=1.5$. The variation in β_F and ν_F between these two regimes strongly suggests that the simple scaling fit (1.2) cannot work over the observed range of flip numbers.

Notice that the probabilities $\rho(F,L)$ are independent of L for the smaller values of F. The smaller events occur totally within the pile and are not affected by its size. In this L-independent region we can fit the data for F greater than about 12 by a power-law form:

$$\rho(F,L)\approx F^{-\delta_F}\ , \tag{2.17}$$

where δ_F is measured to be 1.50 ± 0.05. The other power-law region for higher F values has a different slope on the log-log plot, $\delta_F=2.05\pm0.05$.

In Fig. 6(b) we show the multifractal fits to the unlimited local model. Notice again that there are discrepancies between the curves for values of $\alpha=\log_{10}(F)/\log_{10}(1.5L)$ around 0.7. However, if we employ the same method of data analysis as we used to analyze the limited, local

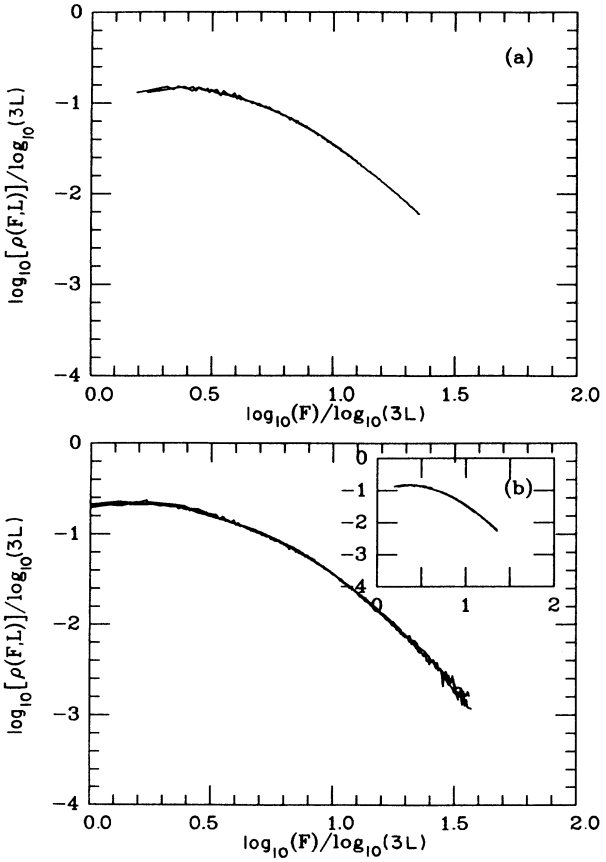

FIG. 3. (a) Same data shown in Fig. 2(d) for $\rho(F,L)$ after removing the data which corresponds to 0 and 1 backward steps of an avalanche. The system sizes are 128 and 512. The multifractal fit is very good. (b) The multifractal fit of $\rho(F,L)$ for the limited local model with $N_F=20$ (L varies from 128 to 2048). The inset in this figure shows a superposition of the f vs α curves for the $N_F=2$ and 20 models. The excellent agreement indicates that these models belong to same universality class.

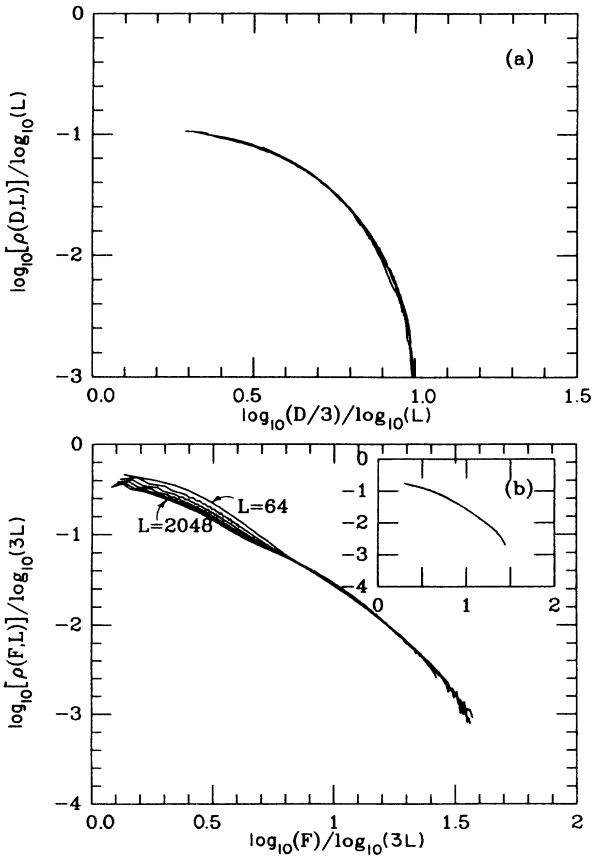

FIG. 4. f vs α curves for the limited nonlocal model with $N_F=2$ (L varies from 64 to 2048). (a) and (b) show the distributions of drop number and flip number, respectively. The inset of (b) shows the data after removal of backward steps 0 and 1.

model (that is, subtract the data for zero and one backward steps of the avalanche) we find the excellent agreement that is shown in the inset. Events with small values of α (i.e., scaling events with relatively smaller flip numbers), can be fit by a power law of the form (2.17), which gives $df(\alpha)/d\alpha = -\delta_F$ in this region. The power law ends in a knee near $\alpha = 1.0$ and then $f(\alpha)$ has another linear region for higher α until α reaches 1.4 or so, whereupon f goes down very rapidly indeed.

In the case of the nonlocal model, it is not possible to do any simple scaling fit for small and intermediate values of F. For large values of F we find exponents which are different from what was found in the local model. If we compare the shapes of the distribution functions for the local and the nonlocal case we see that they are quite different. Whereas the local model has two power-law regimes, the nonlocal model for small values of F does not have any simple scaling behavior.

In Fig. 6(c) we show a multifractal fit for the nonlocal unlimited model. It is a good fit for $F \gg L$. However, it does not work quite as well for small and intermediate values of F where the curves depart from one another near $\alpha = 0.5$. However, as L gets large the differences between the adjacent curves get smaller. We suspect that another microscopic effect may be important for giving rise to these discrepancies. We are currently examining the model to see if this assumption is correct and whether a better multifractal fit could be obtained by removing the correct nonscaling aspects of the data.

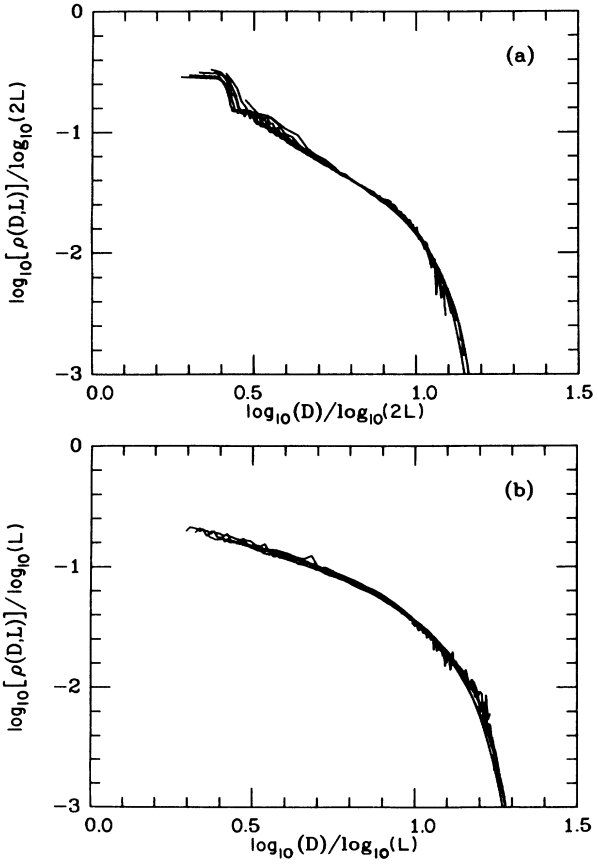

FIG. 5. f vs α curves for the distribution of drop number of (a) unlimited local and (b) the unlimited nonlocal models. (L varies from 32 to 2048.) Equation (2.16) provides a good fit to the data with $\delta_D = 1.66$ for local case and $\delta_D = 0.87$ for nonlocal case.

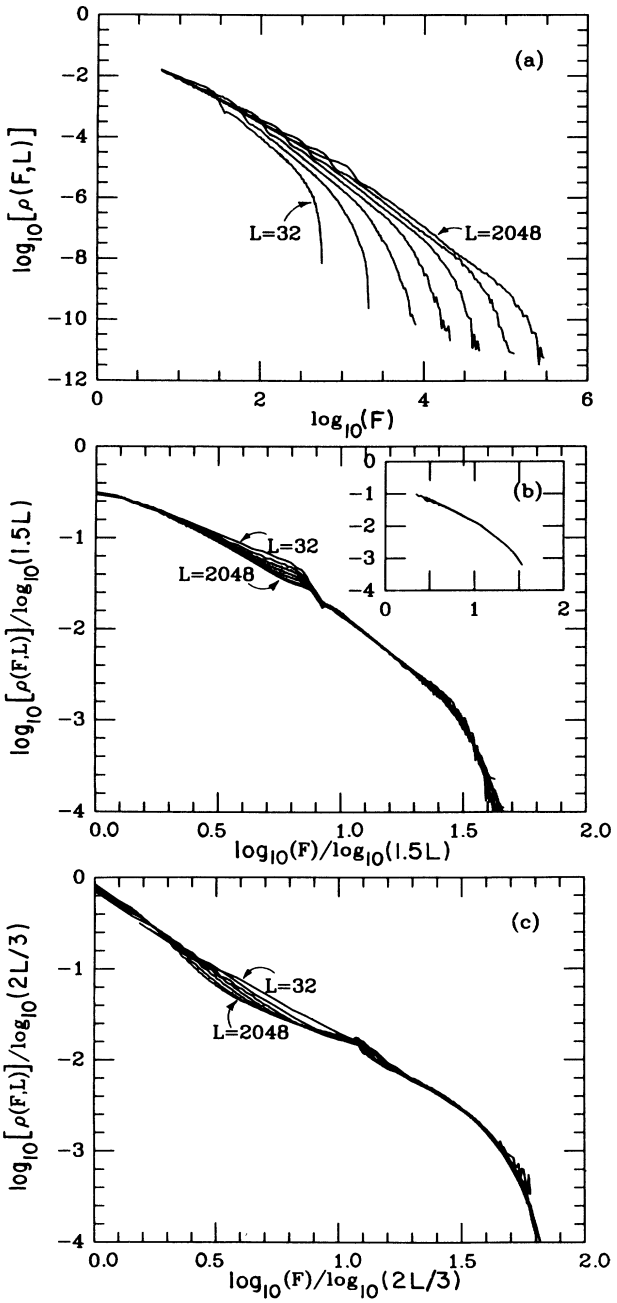

FIG. 6. Finite-size scaling of the distribution of flips for the unlimited models (L varies from 32 to 2048). (a) The local case with exponents ($\beta_F = \nu_F = 0$) chosen to give a good fit for small values of F ($F < L$). (b) The multifractal fit to the unlimited local model. The inset shows the excellent agreement if the data for zero and one backward step of the avalanche are removed. (c) The multifractal fit to the unlimited nonlocal model. L varies between 32 and 2048 in both sets of data.

If we try to summarize our results on these one-dimensional models we see that the multifractal analysis works reasonably well in all cases. Simple scaling seems to work acceptably only in the case of $\rho(D,L)$ for the unlimited models. However, even in these cases, it is not superior to a multifractal fit. It never gives a convincing fit to the data for the flip number. The four different classes of models we have studied appear to fall into four different universality classes. However, in at least one category, the one with limited local rules, two different models showed the same behavior for both the drop and the flip number. This leads us to believe that, even though there is no simple scaling in these models, there is universality.

III. TWO-DIMENSIONAL SIMULATIONS

A. The models

1. General discussion

In this section we extend our simulations from one-dimensional to two-dimensional systems. In each system under study there is a quantity which changes via a nonlinear diffusion process. We are interested in comparing different models to see how the dynamical processes affect such quantities as the distribution of flip numbers [including the exponents of the power-law distribution function, the finite-size-scaling indices, and the $f(\alpha)$ curves]. All our models are basically similar. We limit our consideration to models having the same process for the addition of grains and the same boundary conditions. Our piles are constructed on a two-dimensional square lattice. A randomly chosen site $\mathbf{i}=(x,y)$ is used to start the avalanche. We add one grain to this lattice site according to Eq. (1.1). Once this addition is performed, we check to see whether a slide can occur at any of the lattice sites $\mathbf{i}$. Our models differ from each other in having different criteria for a slide to occur. For all the sites $\mathbf{i}$ which are unstable, we change the height of the piles according to

$$h(\mathbf{i}+\mathbf{r})\rightarrow h(\mathbf{i}+\mathbf{r})-\delta h(\mathbf{r}) \ . \tag{3.1}$$

Here, the exact values of $\delta h(\mathbf{r})$ depend upon the model. For each model, we impose open boundary conditions, which means a grain that moves to the edge of the system can fall off and then not be included in the height anywhere. All our models are local in the sense that the moving grain falls upon a site which is either a nearest neighbor or a next nearest neighbor of the site $\mathbf{i}$.

Even with these limitations, two-dimensional avalanches are more complicated than those in one dimension because each grain has more than one direction in which to move. This complexity is reflected in the two-dimensional dynamical rules through the definition of the condition for an unstable site and the flipping procedure which is called into play once the site is unstable. As in one dimension, the results indicate that there are several different universality classes. [See Table I for a summary of the models considered and of our results for $\rho(F,L)$.] In fact, the scaling-limit outcomes seem to depend upon several aspects of the definition of the models. In what follows we describe two of the features of the model which seem to be relevant, i.e., seem to help define the universality class. The features are the "directedness" of the model and the nature of the "slide criterion."

(i) *Directedness.* There are two different groups of flipping procedures which seem to give quite different results for the average flip number. To describe these rules we use the $\delta h(\mathbf{r})$ defined in Eq. (3.1) to be the change in height at site $\mathbf{r}+\mathbf{i}$ in an elementary slide process, started at site $\mathbf{i}=(x,y)$. One group of flipping procedures satisfies the condition

$$\mathbf{J}=\sum_{\mathbf{r}}\delta h(\mathbf{r})\mathbf{r}=\mathbf{0} \quad \text{(undirected slides)} \tag{3.2a}$$

for each flipping event within the interior of the pile. We call such processes undirected to distinguish them from those in which the basic slide defines a direction, with a vector direction being given by

$$\mathbf{J}=\sum_{\mathbf{r}}\delta h(\mathbf{r})\ \mathbf{r}\neq\mathbf{0} \ \text{(directed slides)} \ . \tag{3.2b}$$

Here, $\mathbf{J}$ is a constant vector which is the same for all slide events occurring within the interior of the pile. We will consider both groups of flipping processes in this section.

The distinction between (3.2a) and (3.2b) is rather similar to the difference between unbiased and biased random walks or between undirected and directed percolation.[9,10] As in random walks, we can expect the behavior to be

TABLE I. A summary of results for $\rho(F,L)$ in the two-dimensional models. $\sigma(x,y)$ gives the criterion for when a site (x,y) is unstable. $\mathbf{J}$ gives the net flow from each unstable site [see Eq. (3.2)]. δ_F, β_F, and ν_F give the scaling indices for each model [see Eqs. (3.10) and (3.13)]. w is the exponent for how the average flip number scales with L [see Eq. (3.3)].

Parameter \ Model	1	2	3	4
$\sigma(x,y)$	$2h(x,y)$ $-h(x+1,y)$ $-h(x,y+1)$	$4h(x,y)-h(x+1,y)$ $-h(x,y+1)-h(x-1,y)$ $-h(x-1,y)$	$h(x,y)$	$h(x,y)$
net flow	$\mathbf{J}\neq\mathbf{0}$	$\mathbf{J}=\mathbf{0}$	$\mathbf{J}\neq\mathbf{0}$	$\mathbf{J}=\mathbf{0}$
w	1.00±0.02	1.9±0.1	1.0 ±0.2	1.9 ±0.1
δ_F	1.35±0.05	1.5±0.1	1.27±0.05	1.05±0.05
β_F	2.3 ±0.1	4.4±0.1	2.2 ±0.1	2.3 ±0.1
ν_F	1.6 ±0.1	3.0±0.1	1.6 ±0.1	2.0 ±0.1

substantially modified whenever the bias is nonzero.

In Sec. II we showed that there was a relationship between the average flip number and the size of the system, for the one-dimensional case. In the limited, local model we found that the relationship was linear, i.e., the power w in

$$\langle F \rangle = \sum_F F\rho(F,L) \sim L^w \tag{3.3}$$

is always unity ($w=1$). This linear relationship arose because a grain moved step by step in one direction until it fell off the end. Now, in our two-dimensional case, we have two possibilities. In our directed models (i.e., those with a net flow in each flipping event), the added particle leaves the system like a biased random walker,[11] so we expect $w=1$. These directed models are thus like those in the one-dimensional cases. On the other hand, for the undirected models, the grains moves like an unbiased random walker, which covers a distance L in L^2 steps. Here F is, of course, the number of steps so that, for undirected models, $w=2$. Thus we expect

$$w = \begin{cases} 2 & \text{for undirected models} \\ 1 & \text{for directed models} \end{cases} \tag{3.4}$$

for very large system size L.

Of course, the actual behavior of our avalanches might, in some situations, be more complicated than that of a random walk, but Eqs. (3.4) at least provide two reasonably simple limiting cases. We shall see that these cases are indeed realized in actual models.

(ii) *Slide criterion.* The definition of an unstable site is different for the various models shown in Table I. On the one hand, we can follow the models initially used by Bak *et al.* and allow a slide to occur whenever the height of a given stack gets bigger than a critical value. In this case the slide criterion is

$$h(x,y) > \sigma_c \quad \text{(critical-height models)} . \tag{3.5a}$$

On the other hand, we can follow the words in the papers of Bak *et al.* and calculate a slope proportional to the difference in heights among the neighboring stacks of the pile. As before, we use the symbol σ to indicate such a slope. Of course, we can choose among several different possible definitions of $\sigma(x,y)$. But whatever we chose, if the quantity is a slope, changing the heights of all nearby piles by a fixed amount should leave $\sigma(x,y)$ invariant. With slope defined in this way, the slide criterion will be

$$\sigma(x,y) > \sigma_c \quad \text{(critical-slope models)} . \tag{3.5b}$$

When the appropriate one of these conditions is satisfied, site (x,y) is unstable and the h's will change through a diffusion process. The last step in defining the model is to define the exact nature of the diffusion by specifying the δh's. Of course, we expect that critical-slope and critical-height models will be in different universality classes since these two kinds of models are sensitive to very different aspects of the local environment on the pile.

We further constrain our models by demanding that grains flow from each unstable site in noncollinear directions. Otherwise we would again have one-dimensional behavior.

2. *Model specification*

The first two two-dimensional models that we study are critical-slope versions of directed and undirected models. For model 1, we define the slope of the pile at site (x,y) as the sum of the height difference of the pile along $+X$ and $+Y$ axis.

$$\sigma(x,y) = 2h(x,y) - h(x+1,y) - h(x,y+1) . \tag{3.6}$$

The unstable grain is limited to flow in either the $+X$ direction or the $+Y$ direction. We have tried two different directed flipping procedures and both of them give the same finite-size-scaling indices for flip and drop number. They are shown in Fig. 7. The arrow in the picture indicates the direction of motion for one grain. Both diffusion processes had net flow pointing in the (1,1) direction in each flipping event.

In model 2, we define a nondirected model with a square symmetry. We let the sum of the height difference along the four lattice directions be our σ,

$$\sigma(x,y) = 4h(x,y) - h(x+1,y) - h(x,y+1) - h(x-1,y) - h(x,y-1) \quad \text{(model 2)} , \tag{3.7}$$

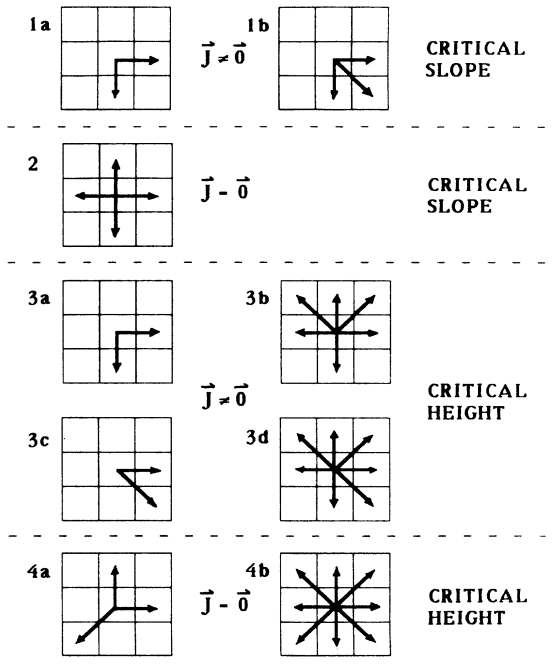

FIG. 7. Diagrams showing how the particles on an unstable site are rearranged in the various two-dimensional models studied in this paper. In each diagram the central site is unstable according to either the critical slope criterion (models 1 and 2) or the critical-height criterion (models 3 and 4). Each arrow in the diagram represents the direction of flow of one grain. **J** is the net flow during each event. If $\mathbf{J}=0$ then the model is called undirected. Otherwise the model is called directed.

and let all unstable sites relax as shown in Fig. 7. Hence $\mathbf{J}=0$ in this model.

Models 3 and 4 follow the idea of the second model in the paper of Bak *et al.* These are critical-height versions of the directed and undirected models. In both models we define the site with $h(x,y)>\sigma_c$ as an unstable site. The rules are chosen so that models 3 and 4 are, respectively, directed and undirected versions of the critical-height model. For each of these models there are several possible ways of defining the flow so as to have the same value of $\mathbf{J}$. The exact laws are shown in Fig. 7.

B. Trivial model

The class of directed models with a critical slope contains models which have an essentially trivial behavior. As in the case of the one-dimensional-pile simulation, we can have a trivial model in which the steady-state behavior puts the entire pile at the critical slope. Then every time a grain is added it will flow to the edge and drop out of the systems. One such trivial model is obtained by defining the slope to be

$$\sigma(x,y)=2h(x,y)-h(x+1,y)-h(x,y+1)\ . \tag{3.8}$$

If σ is greater than σ_c, then the point (x,y) will be unstable and will slide from that point. Our sliding rule is that the unstable point (x,y) will give one grain to the lower one of its two nearest-neighbor sites at $(x+1,y)$ or $(x,y+1)$. If the two neighbors have the same height, then the grain is moved to either site with equal probability. After a large number of steps, the local slope at every site will become σ_c and the shape of the pile will no longer change. The added particles must fall off the system. The distributions of relaxation time and flip number are the same. For example,

$$\rho(F,L)=\begin{cases}\dfrac{2(L-F)+1}{L^2} & \text{for } 1\le F\le L\\ 0 & \text{otherwise}\end{cases} \tag{3.9}$$

for an $L\times L$ square lattice. The drop number is always 1.

C. The nontrivial models: Universality

We stated above that the average flip number would be a useful quantity for sorting out the different universality classes. The values of w, which are the slopes of $\log_{10}\langle F\rangle$ versus $\log_{10}(L)$, are recorded in Table I. The data clearly fall into two different categories. The directed models (1 and 3) have $w\approx 1$. For the undirected models (2 and 4) we find $w\approx 2$. The small deviations of w from what we expected in Models 2 and 4 can be explained by the fact that the sizes of our simulation systems are not large enough. The asymptotic values of w in the four models are consistent with our expected values. From our simulation results, we can confirm our expectation that the directed or undirected nature of the flipping will distinguish different universality classes.

The structure of the probability $\rho(F,L)$ for observing a flip number F in a system of size L is quite different in the two-dimensional case from what we have studied in one dimension. Our data are dominated by a very long region of power-law behavior in which

$$\rho(F,L)=\text{const}\times F^{-\delta_F}\ , \tag{3.10}$$

where the constant is weakly dependent on L for very large L. Figure 8 shows the quality of the power-law fits to the data for one example from each of the four cases. The observed values of δ_F for models 2 and 4 (respectively, $\delta_F=1.5\pm0.1$ and 1.05 ± 0.05) clearly show that these two models are in different universality classes. Models 1 and 3, the directed models, show rather similar behavior (with $\delta_F=1.35\pm0.05$ and 1.27 ± 0.05, respectively) so that we still cannot be sure that they are in different universality classes. Hence we now have good evidence that there are at least three different behaviors among the four models. The only surprise is that models 1 and 3, the two directed models, seem quite similar.

To sharpen our distinctions, we turn to a consideration of the drop number. For all of our models we can get a good fit to the drop-number data for all values of $L\gg 1$ and $D\gg 1$ by using a finite-size-scaling fit of the form

$$\rho(D,L)\sim L^{-\beta_D}g(D/L^{\nu_D})\ . \tag{3.11}$$

Figures 9(a) and 9(b) show log-log plots for the drop-number data of models 1 and 3, respectively. If there were a fit of the form (3.11) all the data would fall upon a single curve. As one can see the single-curve assumption works quite well so that one can reasonably safely use form (3.11) and plots like Fig. 9 to estimate values of β_D and ν_D for the four models. The data for these indices, entered into Table II clearly show that model 1 (with $\nu_D=0.93\pm0.10$) is different from model 3 (which has $\nu_D=0.5\pm0.1$). Hence all four of our models are in different universality classes. On the other hand, the two versions of model 1 have, as far as one can tell, the same behavior in the scaling region of large events and large L. The inset in Fig. 9(a) shows the superposed data for the two versions of model 1. The results certainly do look alike. Hence the models are probably in the same universality class. We find similar universality between the two versions of model 4 and the four versions of model 3.

Notice that there is no small-D straight-line behavior in Fig. 9. Hence generally we cannot, in any meaningful sense, define δ_D.

D. The nontrivial models: Scaling

We also once again check whether a simple size-dependent scaling of the form (3.11) is an adequate description of the data, or whether one might need a multifractal fit. For the drop number the answer seems clear. The simple scaling fit is quite good. One test of this fit is to ask whether the numbers for β_D and ν_D in Table II, which were mostly obtained for the smaller values of D, are consistent with the sum rule (1.5)

$$\sum_D \rho(D,L)D=\langle D\rangle=1\ ,$$

which has substantial contributions from the very largest

D. Equations (1.5) and (3.11) combine to give the constraint

$$\beta_D = 2\nu_D \ . \tag{3.12}$$

Notice that the data in Table II do indeed fit Eq. (3.12). Hence the simple scaling form is certainly acceptable. We also find that multifractal analysis [Eq. (1.3)] works reasonably well for the drop-number distribution $\rho(D,L)$. Nevertheless there were some models (for example, model $1a$) in which this analysis was not quite as good as the simple scaling fit [compare Figs. 10 and 9(a)].

For the distribution of flip number $\rho(F,L)$, we find that the first three models can be well described by the simple finite-size scaling. We can check this by plotting $L^{\beta_F}\rho(F,L)$ versus F/L^{ν_F} to see whether the data points fall onto a single curve and checking the sum rule for $\rho(F,L)$. The simple finite-size-scaling plots are shown in Fig. 8. The distributions of flip number obtained from different size systems do fall onto a single curve in each of the first three models. This fact indicates that for these models $\rho(F,L)$ has the form

$$\rho(F,L) \sim L^{-\beta_F} g(F/L^{\nu_F}) \ . \tag{3.13}$$

Combining this with Eqs. (3.3) and (3.10) we get these relations:

$$\begin{aligned} &2\nu_F - \beta_F = w \ , \\ &\beta_F/\nu_F = \delta_F \ . \end{aligned} \tag{3.14}$$

One can check these relations by using the data shown in Table I and find that for models 1, 2, and 3 the simple finite-size scaling is a very good way to describe the $\rho(F,L)$. In model 1 $g(x)$ has the form

$$g(F/L^{\nu_F}) \sim (F/L^{\nu_F})^{-\delta_F} \exp[-(F/aL^{\nu_F})] \ , \tag{3.15}$$

where a is a constant which is independent of the size L, but varies from model $1a$ to model $1b$. For model 4 $\rho(F,L)$ is a function which shows power-law behavior for $F \le L^2/4$ and then quickly drops to zero. We can superpose the power-law part without any difficulty. However, the simple finite-size scaling does not work well for the tail. This is the reason why the sum-rule relation $2\nu_F - \beta_F = w$ is not satisfied in that model.

The multifractal analysis for the models we study here is also very good. By plotting $\log_{10}[\rho(F,L)]/\log_{10}(L/L_0)$ versus $\log_{10}(F)/\log_{10}(L/L_0)$ we can get a single $f(\alpha)$

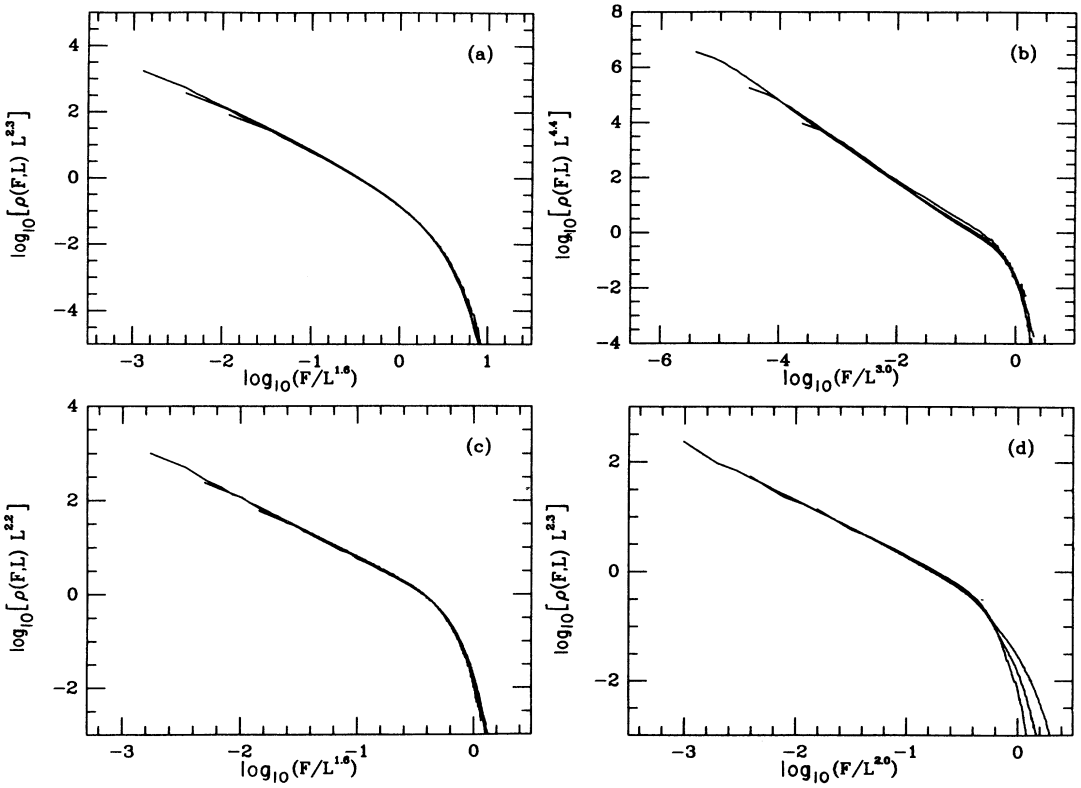

FIG. 8. (a) Finite-size-scaling plots of $\rho(F,L)$ for model $1a$ ($16 \le L \le 64$), (b) model 2 ($16 \le L \le 64$), (c) model $3c$ ($8 \le L \le 64$), and (d) model $4b$ ($8 \le L \le 64$). $\rho(F,L)$ can be fit by power-law distributions with an exponential cutoff at large values of L. In the first three models $\rho(F,L)$ can be described well by the simple finite-size-scaling analysis. The finite-size scaling of $\rho(F,L)$ in model 4 does not fit well. Models 2 and $4b$ have different finite-size-scaling indices for flip number distribution.

curve for different size L in each of models 1, 2, 3, and 4, and we can find that in the last model the multifractal analysis works better than the simple finite-size scaling [compare Figs. 11 and 8(d)].

E. Conclusion

In this section we have shown the results of simulations for several two-dimensional self-organized critical models. From these simulation results we can divide these models into four different universality classes. There are two features relevant to the classification: the directedness of the model and the nature of the slide criterion. Only those models which are in the same universality class have identical finite-size-scaling functions with the same finite-size-scaling indices for both drop-number and flip-number distributions. For all the models we have studied in this section, there are long-range power-law behaviors in the distribution of flip number, but the powers are not the same for all models. These power-law behaviors indicate that the models we study here do have scale-invariant properties and that the analogy between our models and the traditional critical phenomena is acceptable. Finite-size scaling works very well for the drop-number distributions in each model and reasonably well for the flip-number distribution in the first three models. We also find that multifractal analysis gives a good fit to our data. In one case (model 4) it produced a slightly better fit to the flip-number distribution than did the simple scaling analysis. Since both methods of treating the data give comparably good results it is difficult to decide which method is more appropriate.

IV. CONCLUSIONS

In conclusion, we have simulated the behavior of avalanches in one- and two-dimensional models. By studying how the various distribution functions depended on the size of the system, we have been able to investigate the scaling properties of these models and have compared simple finite-size scaling and multifractal analyses of the data. Tang[12] has proposed a hyperscaling argument which suggests that multifractal behavior is more appropriate for these models. By varying the underlying microscopic rules governing an avalanche, we have also studied whether different models have the same universal properties.

In the case of the one-dimensional models we find that multifractal analysis is a much better way to treat the data than the analysis based on simple finite-size scaling. We have also found that these models fall into several different universality classes. Nevertheless there are certain models, with similar (but not identical) rules, which appear to belong to the same class. By contrast, in two

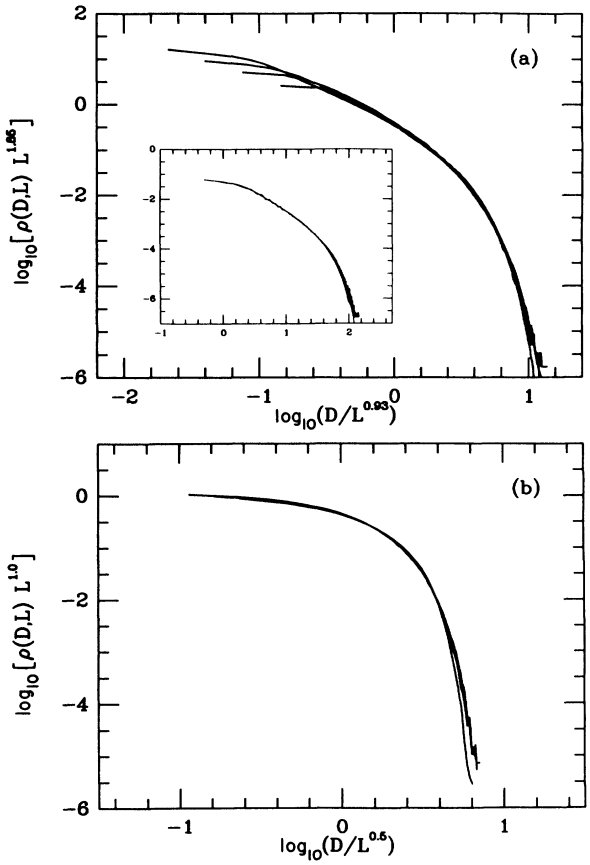

FIG. 9. (a) Finite-size-scaling plot of the drop-number distribution in model 1a ($8 \le L \le 64$) and (b) model 3a ($16 \le L \le 64$). The inset of (a) is the log-log plot of drop-number distributions of models 1a and 1b [which is shifted $-\log_{10}(1.5)$ in the horizontal direction and $\log_{10}(2.25)$ in the vertical direction] obtained from the 32×32 square lattice. From these two figures one can see that the finite-size-scaling indices of the drop-number distribution in models 1a and 3a are not the same.

TABLE II. The finite-size-scaling indices for $\rho(D,L)$ in each of the two-dimensional models. The definitions of β_D and ν_D can be found in Eq. (3.11).

Scaling indices \ Model	1	2	3	4
β_D	1.85±0.10	2.8±0.1	1.0±0.1	1.0±0.1
ν_D	0.93±0.10	1.4±0.1	0.5±0.1	0.5±0.1

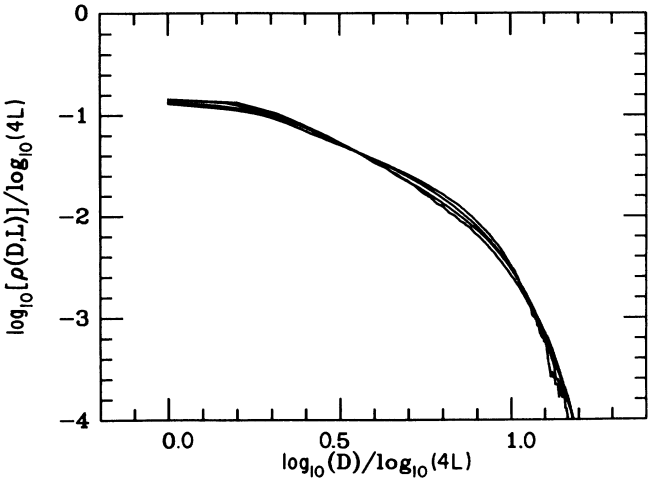

FIG. 10. Multifractal fit of the drop-number distribution for model 1*a* ($8 \leq L \leq 64$).

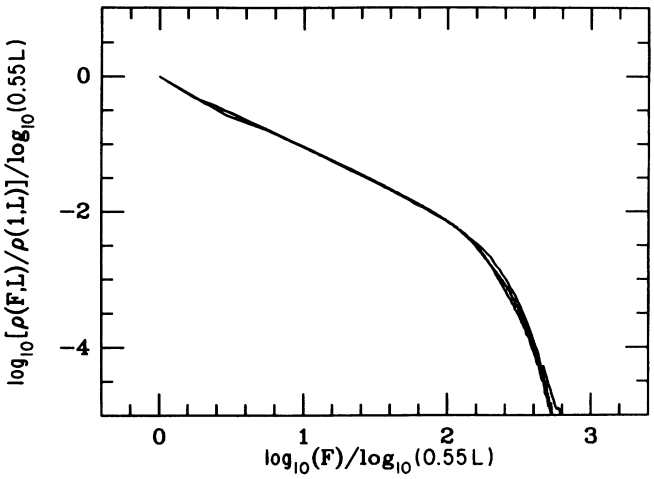

FIG. 11. Multifractal plot of flip-number distribution of model 4*b* ($6 \leq L \leq 64$). Comparing with Fig. 8(d) one sees that, for the case of the flip-number distribution in model 4, the multifractal analysis is better than the finite-size-scaling analysis.

dimensions, we find that the simple finite-size scaling works quite well and that the distribution functions for the flip number can be fit over wide ranges by simple power laws. The multifractal analysis also works well for these two-dimensional models, and it is difficult to tell which form is a better fit to the data. Again, as in one dimension, there are several different universality classes and different models with similar rules belong to the same class.

We therefore conclude that there is evidence for universality in the self-organized critical behavior in these avalanche models. In both one and two dimensions we found evidence for several different universality classes. In contrast to the conclusions of Bak *et al.* the one-dimensional models are far from trivial and have behavior which seems to be more complicated than that found in the two-dimensional systems where finite-size scaling worked very well in most cases. The existence of different universality classes raises the obvious question of how it is possible to classify all of the possible models that exhibit self-organized behavior. Indeed the experiments on real sandpiles indicate that self-organized behavior can include not only critical behavior but behavior reminiscent of a first-order phase transition as well.

ACKNOWLEDGMENTS

We would like to thank P. K. Dixon, G. Grinstein, G. Gunaratne, T. C. Halsey, H. M. Jaeger, A. Libchaber, S. Shenker, C. Tang, K. Wiesenfeld, and T. Witten for useful discussions. We are especially grateful to C-H Liu, who first suggested a nontrivial one-dimensional model. This work was supported in part by National Science Foundation Materials Research Laboratory Grant No. DMR 8519460.

[1]P. Bak, C. Tang, and K. Wiesenfeld, Phys. Rev. Lett. **59**, 381 (1987); Phys. Rev. A **38**, 364 (1988).

[2]C. Tang and P. Bak, Phys. Rev. Lett. **60**, 2347 (1988); J. Stat. Phys. **51**, 797 (1988).

[3]H. M. Jaeger, C-H Liu, and S. R. Nagel, Phys. Rev. Lett. **62**, 40 (1989).

[4]M. E. Fisher, in *Critical Phenomena,* Proceedings of the International School of Physics "Enrico Fermi," Course 51, Varenna, Italy, 1970, edited by M. S. Green (Academic, New York, 1971), p. 1.

[5]M. N. Barber, in *Phase Transitions and Critical Phenomena,* edited by C. Domb and J. L. Lebowitz (Academic, London, 1983), Vol. 8, p. 144.

[6]C. Amitrano, A. Coniglio, and F. di Liberto, Phys. Rev. Lett. **57**, 1016 (1986).

[7]T. C. Halsey, P. Meakin, and I. Procaccia, Phys. Rev. Lett. **56**, 854 (1986).

[8]T. C. Halsey, M. H. Jensen, L. P. Kadanoff, I. Procaccia, and B. I. Shraiman, Phys. Rev. A **33**, 1141 (1986).

[9]L. Kadanoff, in *Phase Transitions and Critical Phenomena,* edited by C. Domb and M. S. Green (Academic, New York, 1976), Vol. 5A, p. 1.

[10]S-K Ma, in *Modern Theory of Critical Phenomena* (Benjamin, New York, 1976).

[11]S. Havlin and D. Ben-Avraham, Adv. Phys. **36**, 695 (1987).

[12]Using a hyperscaling argument Chao Tang (private communication) has found a multifractal description for the probabilities which is slightly different from the $f(\alpha)$ description used here.